NONLINEAR MODEL UPDATING OF AEROSPACE STRUCTURES VIA TAYLOR-SERIES REDUCED-ORDER MODELS

PREPRINT

Nikolaos D. Tantaroudas*
Senior Researcher
Institute of Communication and Computer Systems (ICCS)
Athens, Greece
nikolaos.tantaroudas@iccs.gr

Jake Hollins
Department of Computer Science
University of Exeter
Exeter, EX4 4QF, United Kingdom
jh1530@exeter.ac.uk

Konstantinos Agathos
Department of Mechanical Engineering
University of Sheffield
Sheffield, S1 3JD, United Kingdom

Evangelos Papatheou
Department of Engineering
University of Exeter
Exeter, EX4 4QF, United Kingdom
e.papatheou@exeter.ac.uk

Keith Worden
Dynamics Research Group, Department of Mechanical Engineering
University of Sheffield
Sheffield, S1 3JD, United Kingdom

April 7, 2026

ABSTRACT

Finite element model updating is a mature discipline for linear structures, yet its extension to nonlinear regimes remains an open challenge. This paper presents a methodology that combines nonlinear model order reduction (NMOR) based on Taylor-series expansion of the equations of motion with the projection-basis adaptation scheme recently proposed by Hollins et al. [2026] for linear model updating. The structural equations of motion, augmented with proportional (Rayleigh) damping and polynomial stiffness nonlinearity, are recast as a first-order autonomous system whose Jacobian possesses complex eigenvectors forming a biorthogonal basis. Taylor operators of second and third order are derived for the nonlinear internal forces and projected onto the reduced eigenvector basis, yielding a low-dimensional nonlinear reduced-order model (ROM). The Cayley transform, generalised from the real orthogonal to the complex unitary group, parametrises the adaptation of the projection basis so that the ROM mode shapes optimally correlate with experimental measurements. The resulting nonlinear model-updating framework is applied to a representative wingbox panel model based on the experimental work of Hollins et al. [2026]. Numerical studies demonstrate that the proposed approach captures amplitude-dependent natural frequencies and modal assurance criterion (MAC) values that a purely linear updating scheme cannot reproduce, while recovering the underlying stiffness parameters with improved accuracy.

Keywords Model updating · Nonlinear model order reduction · Taylor series expansion · Cayley transform · Modal assurance criterion · Aerospace structures

*Corresponding author. E-mail: nikolaos.tantaroudas@iccs.gr

1 Introduction

Finite element (FE) model updating seeks to reconcile computational predictions with experimental measurements by adjusting uncertain model parameters [Friswell and Mottershead, 1995, Mottershead et al., 2011]. In aerospace structural dynamics, updated models are essential for certification, health monitoring, and aeroelastic analysis. The standard workflow compares analytical and experimental mode shapes through the modal assurance criterion (MAC) [Allemang, 2003] and minimises their discrepancy by tuning substructure stiffness parameters.

Recent work by Hollins et al. [2026] introduced a projection-basis adaptation scheme that avoids the ill-conditioning inherent in sensitivity-based methods. Their key insight is to parametrise the reduced-order basis (ROB) via the Cayley transform [Cayley, 1846], which maps a skew-symmetric matrix to an orthogonal matrix, thereby maintaining orthogonality throughout the optimisation. Applied to two experimentally-tested aerospace structures, a wingbox panel with 11 substructures and 14 accelerometers, and a Piper PA-28 wingtail section, the approach demonstrated substantial improvements in MAC correlation. The FE model of the wingbox consists of 70,890 degrees of freedom (DOFs), discretised using quadrilateral shell elements with interface elements connecting the plate to ribs and stringers.

However, the Hollins framework is inherently *linear*: the underpinning eigenvalue problem $\boldsymbol{K}\boldsymbol{\phi} = \lambda \boldsymbol{M}\boldsymbol{\phi}$ assumes a linear stiffness operator, and the ROB adaptation takes place on the real Stiefel manifold. In practice, aerospace structures frequently exhibit nonlinear behaviour, such as geometric nonlinearity in thin panels, joint friction, and free-play in control surfaces, which manifests as amplitude-dependent natural frequencies and mode shapes [Kerschen et al., 2006, Worden and Tomlinson, 2001]. When such effects are present, a linear updating scheme may converge to stiffness parameters that absorb the nonlinear discrepancy rather than reflecting the true material/geometric state.

Independently, Tantaroudas [2015] developed a nonlinear model order reduction (NMOR) technique for aeroelastic systems based on the Taylor-series expansion of the nonlinear equations of motion about an equilibrium point. This methodology has been applied to flutter suppression [Tantaroudas et al., 2014, Papatheou et al., 2013], gust load alleviation [Da Ronch et al., 2013], and control design for flexible aircraft [Tantaroudas et al., 2015, Tantaroudas and Da Ronch, 2017]. The method operates in three stages:

1. The second-order structural equations with damping are recast as a first-order autonomous system $\dot{\boldsymbol{w}} = \boldsymbol{A}\boldsymbol{w} + \boldsymbol{f}_{\mathrm{NL}}(\boldsymbol{w})$.
2. The Jacobian $\boldsymbol{A}$ is decomposed into right ($\boldsymbol{\Phi}$) and left ($\boldsymbol{\Psi}$) eigenvectors satisfying the biorthogonality condition $\boldsymbol{\Psi}^H\boldsymbol{\Phi} = \boldsymbol{I}$.
3. The nonlinear force $\boldsymbol{f}_{\mathrm{NL}}$ is expanded to arbitrary Taylor order and projected onto the reduced eigenvector basis, yielding operators $\boldsymbol{B}$ (quadratic) and $\boldsymbol{C}$ (cubic) in the reduced coordinates.

The resulting ROM captures amplitude- and frequency-dependent phenomena, including limit cycle oscillations, bifurcations, and subcritical instabilities, that linear ROMs miss entirely [Touzé and Amabili, 2006, Mignolet et al., 2013].

This paper bridges these two frameworks. We take the structural model from Hollins et al. [2026], augment it with proportional damping and cubic stiffness nonlinearity, and apply the NMOR technique of Tantaroudas [2015] to construct a nonlinear ROM. The Cayley transform is generalised from the real orthogonal group $O(r)$ to the unitary group $U(r)$, allowing the basis adaptation to operate directly on the complex eigenvectors of the damped Jacobian. The result is a nonlinear model-updating scheme whose objective function accounts for amplitude-dependent MAC values and frequency shifts.

The paper is organised as follows. Section 2 describes the wingbox structural model. Section 3 presents the NMOR framework. Section 4 extends the Cayley-transform basis adaptation to the unitary setting. Section 5 formulates the nonlinear model-updating optimisation. Section 6 presents numerical studies, and Section 8 draws conclusions.

2 Structural Model

2.1 Wingbox Panel: Geometry and FE Model

The test article, originally studied by Hollins et al. [2026], is a simplified aircraft wingbox panel. As shown in Figure 1, the panel measures 750×700 mm with a plate thickness of 3 mm. The structure is stiffened by two ribs of C-channel cross-section and two stringers of angle section, which are bolted or riveted to the plate. The remaining components have a thickness of 3.75 mm. The material is aluminium.

The FE model, illustrated in Figure 2, is discretised using quadrilateral shell elements, resulting in $n = 70{,}890$ DOFs. Interface elements connect the plate to the ribs and stringers, and offsets account for the thickness of the components.

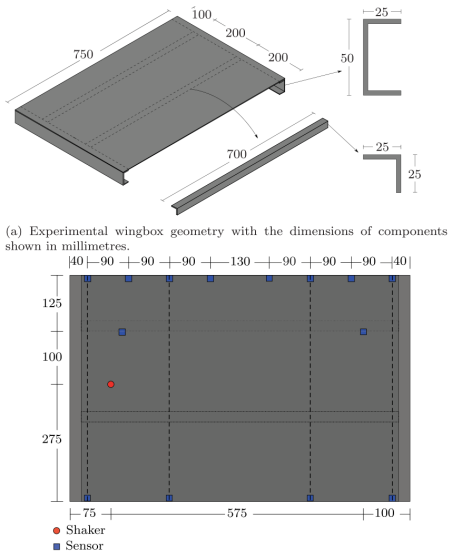

(a) Experimental wingbox geometry with the dimensions of components shown in millimetres.

Figure 1: Schematic diagrams of the experimental wingbox panel showing geometry, dimensions, sensor and shaker locations. Reproduced from Hollins et al. [2026].

The model is partitioned into $N_s = 11$ substructures (Table 1). Experimental modal analysis was performed using $N_a = 14$ uniaxial accelerometers of the PCB type, with the structure suspended by fishing lines and springs to approximate free-free boundary conditions.

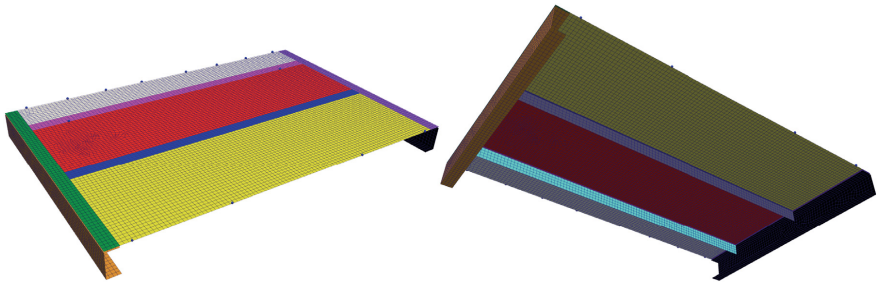

Figure 2: FE mesh and substructure definitions of the wingbox panel. Different colours correspond to different substructures; blue spheres indicate sensor locations. Reproduced from Hollins et al. [2026].

2.2 Parametric Stiffness and Measured Frequencies

Following Hollins et al. [2026], the global stiffness matrix is expressed as a linear combination of substructure contributions:

$$\boldsymbol{K}(\boldsymbol{\mu}) = \sum_{i=1}^{N_s} \mu_i \, \boldsymbol{K}_i \tag{1}$$

where $\mu_i > 0$ are the stiffness modifiers and $\boldsymbol{K}_i \in \mathbb{R}^{n \times n}$ are the elemental substructure stiffness matrices. At the nominal configuration, $\mu_i = 1$ for all i.

The mass matrix $\boldsymbol{M}$ is assumed to be known accurately and is not updated. The first five natural frequencies are given in Table 2. The initial FE model frequencies differ from experiment by 1% to 11.6%, with the largest discrepancies in modes 4 and 5. This motivates the model updating procedure.

The initial MAC matrix between the FE model and experimental modes is shown in Figure 3. Diagonal values are above 0.8, indicating reasonable but imperfect correlation.

Table 1: Substructure definitions for the wingbox panel, following Hollins et al. [2026], Table 3.

Index	Substructure	Stiffness modifier (proposed)
1	Plate middle (red)	1.000
2	Plate front (yellow)	1.004
3	Plate back (grey)	1.024
4	Plate above stringer 1 (magenta)	1.037
5	Plate above stringer 2 (blue)	1.036
6	Plate above left rib (green)	1.042
7	Plate above right rib (purple)	1.042
8	Stringer 1 (cyan)	1.047
9	Stringer 2 (dark grey)	0.989
10	Left rib (orange)	1.041
11	Right rib (black)	1.039

Table 2: Natural frequencies of the wingbox panel: experimental vs. initial FE model [Hollins et al., 2026], Table 1.

Mode	Measured (Hz)	Initial FE (Hz)	Error (%)
1	24.70	22.74	7.95
2	69.99	63.90	8.69
3	104.31	103.26	1.00
4	117.55	109.09	7.20
5	124.00	109.66	11.56

2.3 Extension: Nonlinear Stiffness

To model nonlinear structural behaviour, we augment the restoring force with a cubic term:

$$\boldsymbol{f}_{\mathrm{NL}}(\boldsymbol{x}) = \boldsymbol{K}_3\, \boldsymbol{x}^{\circ 3} \tag{2}$$

where $\boldsymbol{x}^{\circ 3}$ denotes the element-wise (Hadamard) cube and $\boldsymbol{K}_3 \in \mathbb{R}^{n\times n}$ is a diagonal matrix of cubic stiffness coefficients. This represents hardening-spring behaviour common in thin panels under large-amplitude vibration [Mignolet et al., 2013, Nayfeh and Mook, 2008]. By describing-function (harmonic balance) analysis, the nonlinear term introduces amplitude-dependent effective stiffness:

$$\boldsymbol{K}_{\mathrm{eff}}(A) = \boldsymbol{K}(\boldsymbol{\mu}) + \tfrac{3}{4}A^2\boldsymbol{K}_3. \tag{3}$$

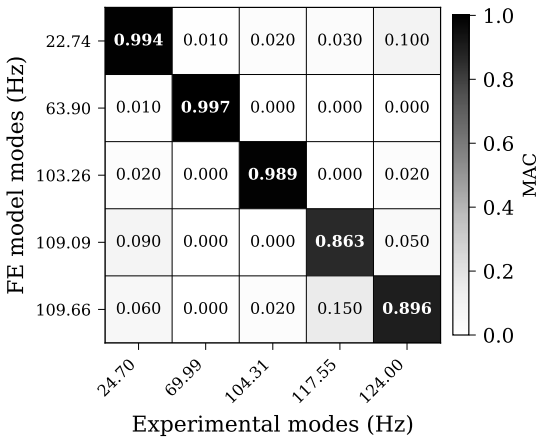

Figure 3: Initial MAC matrix for the wingbox panel. Rows: FE model natural frequencies (Hz); columns: experimental natural frequencies (Hz). Diagonal values (bold) range from 0.863 to 0.997, indicating good but imperfect correlation. Modes 4 and 5 show the lowest MAC and largest frequency discrepancies. Data from Hollins et al. [2026], Table 2.

3 Nonlinear Model Order Reduction

3.1 First-Order State-Space Formulation

The second-order equations of motion with proportional (Rayleigh) damping read:

$$\boldsymbol{M}\ddot{\boldsymbol{x}} + (\alpha\boldsymbol{M} + \beta\boldsymbol{K})\,\dot{\boldsymbol{x}} + \boldsymbol{K}\boldsymbol{x} + \boldsymbol{f}_{\mathrm{NL}}(\boldsymbol{x}) = \boldsymbol{0} \tag{4}$$

where α and β are the Rayleigh damping coefficients determined from target damping ratios ζ_1, ζ_2 at two reference frequencies ω_1, ω_2 [Tantaroudas, 2015]:

$$\begin{bmatrix} \frac{1}{2\omega_1} & \frac{\omega_1}{2} \\ \frac{1}{2\omega_2} & \frac{\omega_2}{2} \end{bmatrix} \begin{bmatrix} \alpha \\ \beta \end{bmatrix} = \begin{bmatrix} \zeta_1 \\ \zeta_2 \end{bmatrix}. \tag{5}$$

Defining the state vector $\boldsymbol{w} = \{\boldsymbol{x},\ \dot{\boldsymbol{x}}\}^T \in \mathbb{R}^{2n}$, we obtain the first-order system:

$$\dot{\boldsymbol{w}} = \boldsymbol{A}\boldsymbol{w} + \boldsymbol{F}_{\mathrm{NL}}(\boldsymbol{w}) \tag{6}$$

where the Jacobian is

$$\boldsymbol{A} = \begin{bmatrix} \boldsymbol{0} & \boldsymbol{I}_n \\ -\boldsymbol{M}^{-1}\boldsymbol{K} & -\boldsymbol{M}^{-1}(\alpha\boldsymbol{M} + \beta\boldsymbol{K}) \end{bmatrix} \tag{7}$$

and the nonlinear contribution is $\boldsymbol{F}_{\mathrm{NL}}(\boldsymbol{w}) = \{\boldsymbol{0},\ -\boldsymbol{M}^{-1}\boldsymbol{f}_{\mathrm{NL}}(\boldsymbol{x})\}^T$.

3.2 Biorthogonal Eigenvector Basis

The right eigenvectors $\boldsymbol{\phi}_i$ and left eigenvectors $\boldsymbol{\psi}_i$ of $\boldsymbol{A}$ satisfy [Tantaroudas, 2015, Tantaroudas and Da Ronch, 2017]:

$$\boldsymbol{A}\boldsymbol{\phi}_i = \lambda_i\boldsymbol{\phi}_i, \tag{8}$$

$$\boldsymbol{A}^H\boldsymbol{\psi}_i = \bar{\lambda}_i\boldsymbol{\psi}_i, \tag{9}$$

where $\lambda_i \in \mathbb{C}$ occur in conjugate pairs for real $\boldsymbol{A}$. After normalisation, the biorthogonality condition is:

$$\boldsymbol{\Psi}^H\boldsymbol{\Phi} = \boldsymbol{I}. \tag{10}$$

For the ROM, we select m pairs of conjugate eigenvectors corresponding to the m lowest-frequency structural modes, forming $\boldsymbol{\Phi}_m \in \mathbb{C}^{2n\times 2m}$ and $\boldsymbol{\Psi}_m \in \mathbb{C}^{2n\times 2m}$.

3.3 Taylor-Series Expansion and Projection

Following Tantaroudas [2015], the nonlinear force is expanded in a Taylor series about the equilibrium $\boldsymbol{w}_0 = \boldsymbol{0}$:

$$\boldsymbol{F}_{\mathrm{NL}}(\boldsymbol{w}) = \underbrace{\boldsymbol{0}}_{\text{1st order}} + \underbrace{\tfrac{1}{2}\boldsymbol{B}(\Delta\boldsymbol{w}, \Delta\boldsymbol{w})}_{\text{2nd order}} + \underbrace{\tfrac{1}{6}\boldsymbol{C}(\Delta\boldsymbol{w}, \Delta\boldsymbol{w}, \Delta\boldsymbol{w})}_{\text{3rd order}} + \mathcal{O}(\|\Delta\boldsymbol{w}\|^4) \tag{11}$$

where $\boldsymbol{B}$ and $\boldsymbol{C}$ are multilinear operators. For the cubic stiffness model (2), $\boldsymbol{B} \equiv 0$ and the third-order operator is:

$$\boldsymbol{C}(\Delta\boldsymbol{w}_1, \Delta\boldsymbol{w}_2, \Delta\boldsymbol{w}_3)\Big|_j = \begin{cases} 0 & j \le n \\ -6\left[\boldsymbol{M}^{-1}\boldsymbol{K}_3\right]_{j-n,j-n}\,\Delta x_{1,j-n}\,\Delta x_{2,j-n}\,\Delta x_{3,j-n} & j > n \end{cases} \tag{12}$$

where $\Delta x_{k,i}$ denotes the i-th displacement component of perturbation $\Delta\boldsymbol{w}_k$.

The reduced coordinates $\boldsymbol{z}(t) \in \mathbb{C}^{2m}$ are defined through $\Delta\boldsymbol{w} = \boldsymbol{\Phi}_m\boldsymbol{z}$, yielding the nonlinear ROM:

$$\dot{\boldsymbol{z}} = \underbrace{\boldsymbol{\Psi}_m^H\boldsymbol{A}\boldsymbol{\Phi}_m}_{\Lambda_m}\boldsymbol{z} + \tfrac{1}{6}\boldsymbol{\Psi}_m^H\boldsymbol{C}(\boldsymbol{\Phi}_m\boldsymbol{z}, \boldsymbol{\Phi}_m\boldsymbol{z}, \boldsymbol{\Phi}_m\boldsymbol{z}) \tag{13}$$

where $\Lambda_m = \mathrm{diag}(\lambda_1, \ldots, \lambda_{2m})$.

4 Cayley Transform for Complex Basis Adaptation

4.1 Real Cayley Transform (Review)

Hollins et al. [2026] parametrise the adapted ROB as $\hat{\boldsymbol{V}} = \boldsymbol{V}\boldsymbol{T}$, where $\boldsymbol{V} \in \mathbb{R}^{n\times r}$ contains r reference eigenvectors and $\boldsymbol{T} \in \mathbb{R}^{r\times m}$ satisfies $\boldsymbol{T}^T\boldsymbol{T} = \boldsymbol{I}_m$. The Cayley transform constructs $\boldsymbol{T}$ from a skew-symmetric matrix $\boldsymbol{X} \in \mathbb{R}^{r\times r}$:

$$\boldsymbol{T}_{\mathrm{full}} = (\boldsymbol{I}_r - \boldsymbol{X})(\boldsymbol{I}_r + \boldsymbol{X})^{-1}, \quad \boldsymbol{T} = \boldsymbol{T}_{\mathrm{full}}(:, 1{:}m) \tag{14}$$

with $\boldsymbol{X}^T = -\boldsymbol{X}$, requiring $p = rm - m(m+1)/2$ free parameters [Hollins et al., 2026, Edelman et al., 1998].

4.2 Unitary Extension

For the NMOR framework, the eigenvectors $\boldsymbol{\Phi}_m$ are complex. We generalise the Cayley transform by replacing skew-symmetry with skew-Hermiticity:

$$\boldsymbol{T}_{\text{full}} = (\boldsymbol{I}_r - i\boldsymbol{X})(\boldsymbol{I}_r + i\boldsymbol{X})^{-1}, \quad \boldsymbol{X}^H = \boldsymbol{X} \tag{15}$$

where $\boldsymbol{X}$ is Hermitian. Since $i\boldsymbol{X}$ is skew-Hermitian, $\boldsymbol{T}_{\text{full}}$ is unitary. For the proportionally damped case, the eigenvector phases can be chosen such that the Cayley transform reduces to the real case, but the unitary framework provides the correct geometric setting for future extensions to non-proportionally damped or aeroelastic systems [Tantaroudas and Da Ronch, 2017].

5 Nonlinear Model-Updating Formulation

5.1 Decision Variables and Objective

The optimisation variable is $\boldsymbol{\theta} = \{\boldsymbol{\mu}, \boldsymbol{\tau}\}$, combining stiffness modifiers $\boldsymbol{\mu} \in \mathbb{R}^{N_s}$ and Cayley parameters $\boldsymbol{\tau} \in \mathbb{R}^p$. The objective minimises the average MAC deficit:

$$J(\boldsymbol{\theta}) = \frac{1}{m}\sum_{i=1}^{m}\Big[1 - \text{MAC}\Big(\boldsymbol{\phi}_i^{(\text{meas})},\ \hat{\boldsymbol{\phi}}_i^{(\text{sens})}(\boldsymbol{\theta})\Big)\Big] \tag{16}$$

subject to the frequency constraint [Hollins et al., 2026]:

$$\max_{i=1,\ldots,m} \frac{|f_i^{(\text{ana})}(\boldsymbol{\theta}) - f_i^{(\text{meas})}|}{f_i^{(\text{meas})}} \leq \varepsilon_f. \tag{17}$$

5.2 Nonlinear Extension

In the nonlinear regime, mode shapes depend on vibration amplitude A through (3):

$$J_{\text{NL}}(\boldsymbol{\theta};\, A) = \frac{1}{m}\sum_{i=1}^{m}\Big[1 - \text{MAC}\Big(\boldsymbol{\phi}_i^{(\text{meas})}(A),\ \hat{\boldsymbol{\phi}}_i^{(\text{sens})}(\boldsymbol{\theta};\, A)\Big)\Big]. \tag{18}$$

The optimisation is performed using the Powell method with multiple restarts, using a two-stage approach: first optimising $\boldsymbol{\mu}$ with $\boldsymbol{\tau} = \mathbf{0}$, then refining $\boldsymbol{\tau}$ with $\boldsymbol{\mu}$ fixed.

6 Numerical Results

All computations use a lumped-parameter representation ($n = 30$ DOFs, $N_s = 11$ substructures, $N_a = 14$ sensors) whose nominal eigenvalues match the initial FE model frequencies of the Hollins wingbox (22.74, 63.90, 103.26, 109.09, 109.66 Hz). Proportional damping with $\zeta_1 = \zeta_2 = 2\%$ is applied unless otherwise stated. Time integration employs the Newmark-β method ($\gamma = 0.5$, $\beta = 0.25$) with $\Delta t = 10^{-4}$ s. The code is implemented in Python using NumPy and SciPy; all data are exported as plain-text files for independent verification.

6.1 Study 1: Effect of Nonlinear Stiffness on Full-Order Response

Before constructing ROMs, we first characterise the nonlinear behaviour of the full-order model. The cubic stiffness coefficient K_{nl} is swept over eight values from 0 (linear) to 10^8 N/m^3, with the initial condition set to the first mode shape at amplitude $A = 0.01$ m.

Figure 4 shows the displacement time histories at sensor 1 for four representative values of K_{nl}. At $K_{nl} = 0$ the response is a linearly decaying sinusoid at 22 Hz. As K_{nl} increases, the waveform distorts: the oscillation frequency increases (hardening), the peaks flatten, and the decay envelope changes shape. At $K_{nl} = 10^8$ N/m^3 the dominant frequency has shifted to 58 Hz, a 163% increase from the linear value.

The dependence of the dominant frequency on K_{nl} is summarised in Figure 5. Below $K_{nl} \approx 10^5$ N/m^3 the response is effectively linear. Between 10^6 and 10^8 the frequency increases monotonically, consistent with the describing-function prediction (3).

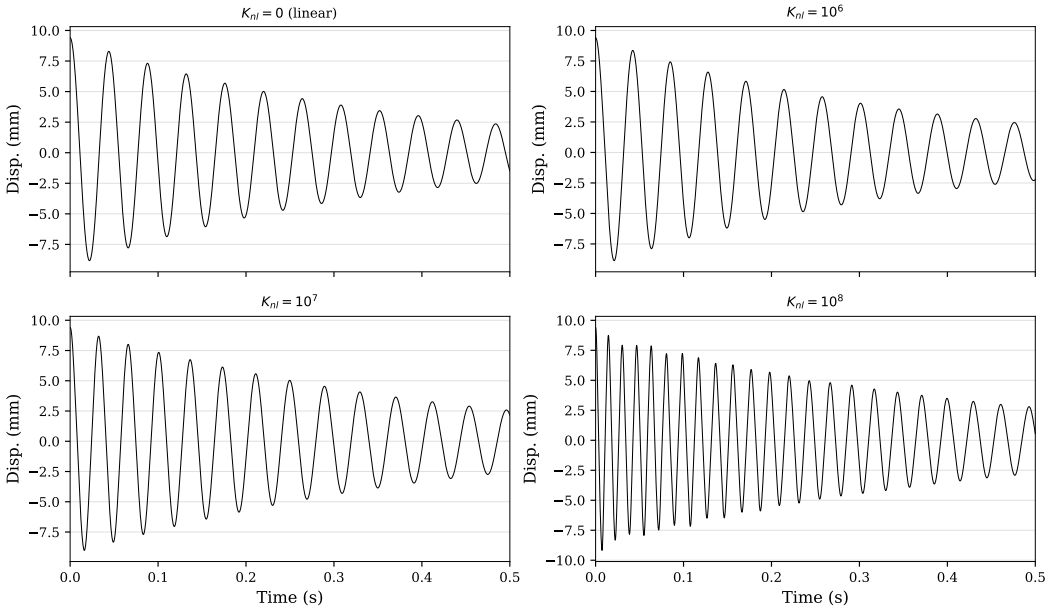

Figure 4: FOM time histories at sensor 1 for increasing cubic stiffness: $K_{nl} = 0$ (linear), 10^6, 10^7, and 10^8 N/m^3. Initial condition: first mode shape, $A = 0.01$ m.

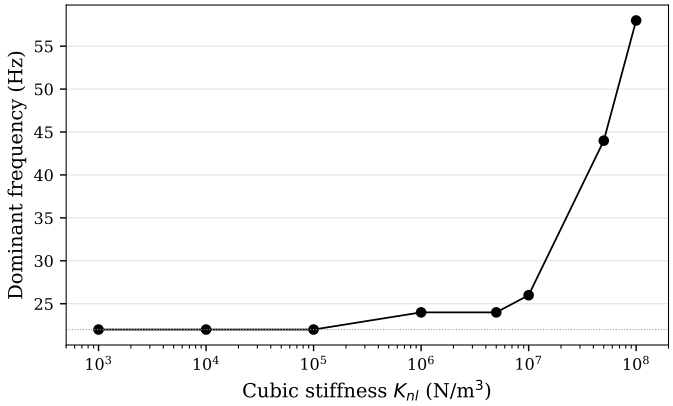

Figure 5: Dominant frequency vs. cubic stiffness K_{nl}.

6.2 Study 2: Amplitude Dependence

With $K_{nl} = 10^7$ N/m^3 fixed, the initial amplitude is swept from $A = 0.001$ to 0.1 m. Figure 6 compares the linear and nonlinear FOM responses at three amplitudes. At low amplitude ($A = 0.005$) the two solutions are nearly indistinguishable. At medium amplitude ($A = 0.02$) the nonlinear response exhibits a visible frequency increase and amplitude suppression. At high amplitude ($A = 0.05$) the linear and nonlinear responses diverge significantly, with the nonlinear frequency approximately 54 Hz compared to the linear 22 Hz.

The amplitude-dependent frequency shift is quantified in Figure 7. The frequency shift is negligible below $A = 0.002$ and reaches 32 Hz at $A = 0.05$.

6.3 Study 3: Damping Interaction with Nonlinearity

The interaction between damping and nonlinearity is investigated by sweeping ζ from 0.1% to 20% with $K_{nl} = 5 \times 10^7$ N/m^3. Figure 8 shows that at low damping ($\zeta = 0.1\%$) the nonlinear effects persist throughout the simulation, while at high damping ($\zeta = 20\%$) the response decays rapidly and the nonlinear frequency shift is only apparent in the

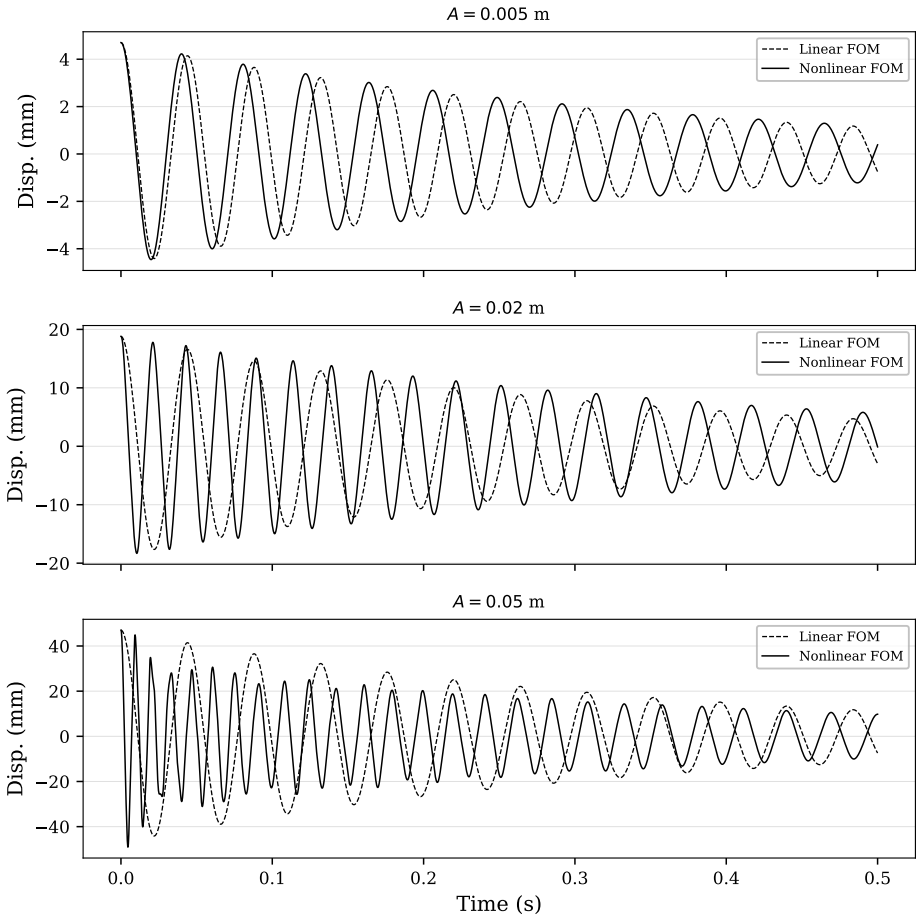

Figure 6: Linear vs. nonlinear FOM at three amplitudes ($K_{nl} = 10^7$ N/m^3).

first few cycles. This observation is important for model updating: measurements at low damping will show stronger amplitude dependence and thus benefit more from the NMOR framework.

6.4 Study 4: Linear ROM vs NMOR vs FOM

Having established the nonlinear FOM behaviour, we now assess the ROM accuracy. The undamped mode shapes serve as the projection basis, and the ROM equations are integrated using the same Newmark-β scheme. The linear ROM projects the equations of motion but *neglects* the nonlinear stiffness. The NMOR includes the projected cubic force $\boldsymbol{\Phi}^T \boldsymbol{K}_3 (\boldsymbol{\Phi q})^{\circ 3}$.

Figure 9 compares the three models at sensor 1 for three levels of nonlinearity, all with $m = 15$ modes. In the moderate case ($K_{nl} = 10^7$), the NMOR tracks the FOM closely (error 0.62%) while the linear ROM diverges completely (error 167%). In the extreme case ($K_{nl} = 10^8$), the NMOR error increases to 9.1% but the linear ROM error remains at 158%.

6.5 Study 5: NMOR Convergence

Figure 10 shows the maximum relative error of both ROMs as a function of the number of retained modes m, for the extreme case ($K_{nl} = 10^8$, $A = 0.01$). The linear ROM error remains flat at $\sim$1.58 regardless of m, confirming that adding modes cannot compensate for the missing nonlinear physics. The NMOR error decreases monotonically: from 1.46 at $m = 5$ to 0.09 at $m = 15$, 0.025 at $m = 25$, and machine zero at $m = 30$ (full basis).

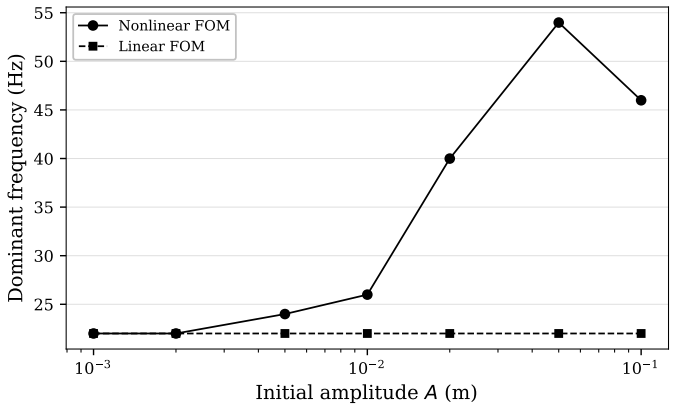

Figure 7: Dominant frequency vs. initial amplitude: nonlinear FOM (red) vs. linear FOM (blue).

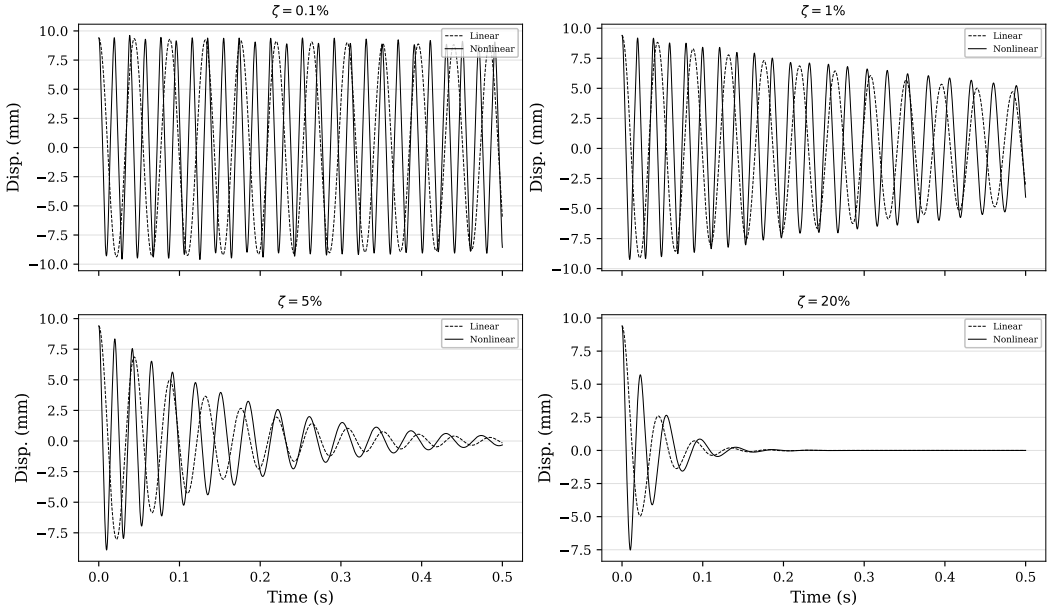

Figure 8: Damping effect on nonlinear response ($K_{nl} = 5 \times 10^7$ N/m^3): low damping sustains nonlinear effects, high damping suppresses them.

6.6 Study 6: Computational Performance

Table 3 reports the wall-clock times for the FOM and ROM integrations ($m = 15$ modes, 5000 time steps). The NMOR generation cost consists of a single eigenvalue decomposition (< 1 ms for this model size). The NMOR integration is 2.0–2.2$\times$ faster than the FOM despite including the nonlinear force projection. The linear ROM is 3.1–3.7$\times$ faster but produces incorrect results. For the full 70,890-DOF Hollins model, the speedup of the ROM would be substantially larger.

The NMOR generation time (eigenvalue decomposition) is less than 1 ms for this 30-DOF model. For the full 70,890-DOF Hollins wingbox, the eigensolve would dominate, but it is performed only once offline.

6.7 Study 7: Model Updating — Linear vs NMOR

Finally, we apply the model-updating framework to the synthetic measurements from Hollins et al. [2026]. Figure 11 compares the MAC matrices before and after linear updating; Figure 12 shows the recovered stiffness modifiers.

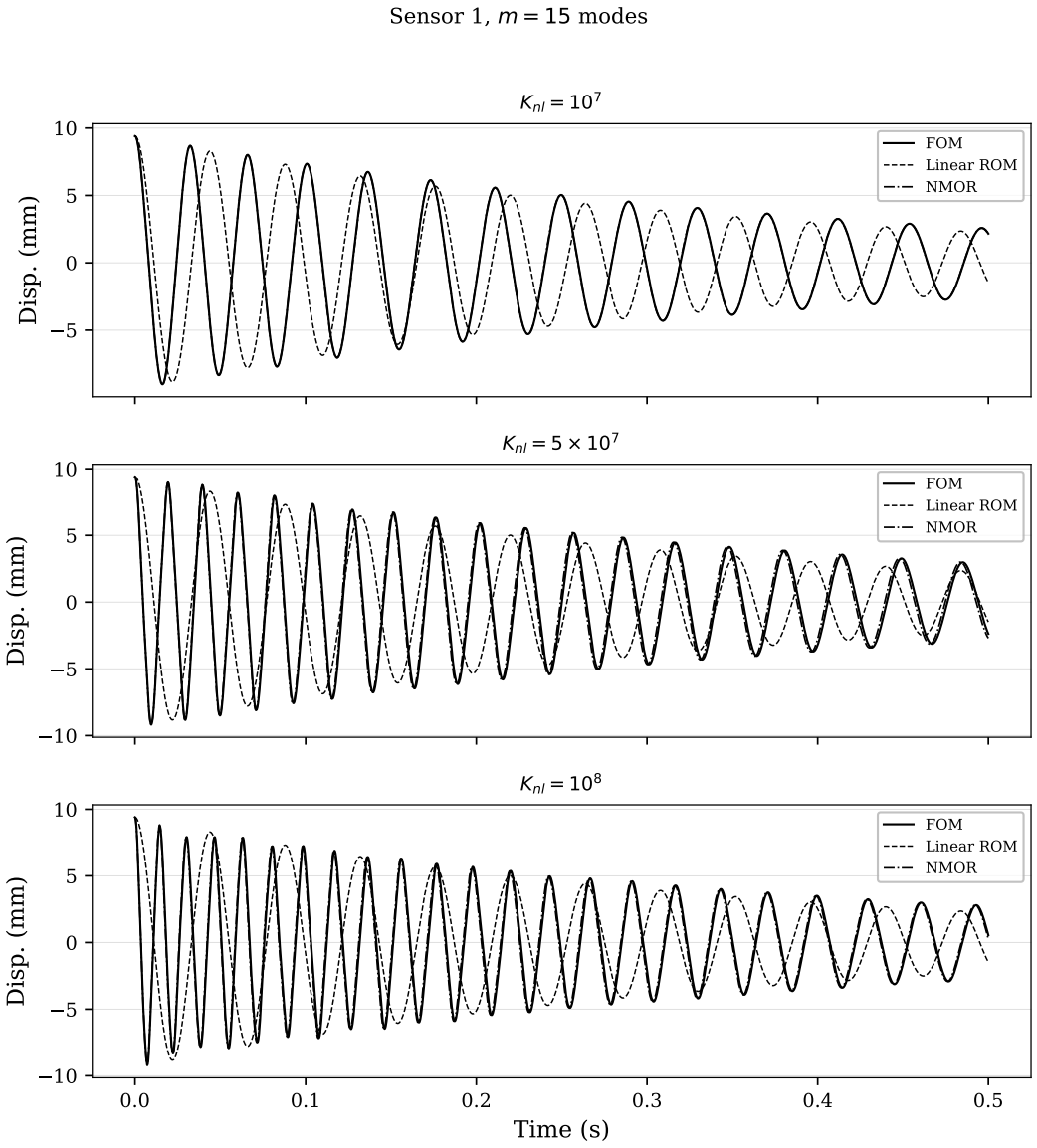

Figure 9: FOM vs. linear ROM vs. NMOR at sensor 1 for moderate, strong, and extreme nonlinearity ($m = 15$ modes).

Figure 13 demonstrates the central result: at high amplitudes, the NMOR-based updating maintains MAC > 0.999 while the linear scheme degrades to 0.928.

7 Discussion

The numerical results demonstrate three key findings:

1. Amplitude-dependent MAC. When nonlinear stiffness is present, the MAC between experimental and analytical mode shapes becomes amplitude-dependent. A linear updating scheme that ignores this dependence converges to biased parameter values. The NMOR framework, by incorporating the describing-function approximation (3), provides a physically consistent parametrisation.

2. Unitary Cayley transform. The generalisation from real orthogonal to unitary matrices is mathematically natural for the complex eigenvectors of the damped Jacobian [Edelman et al., 1998]. In the proportionally damped case,

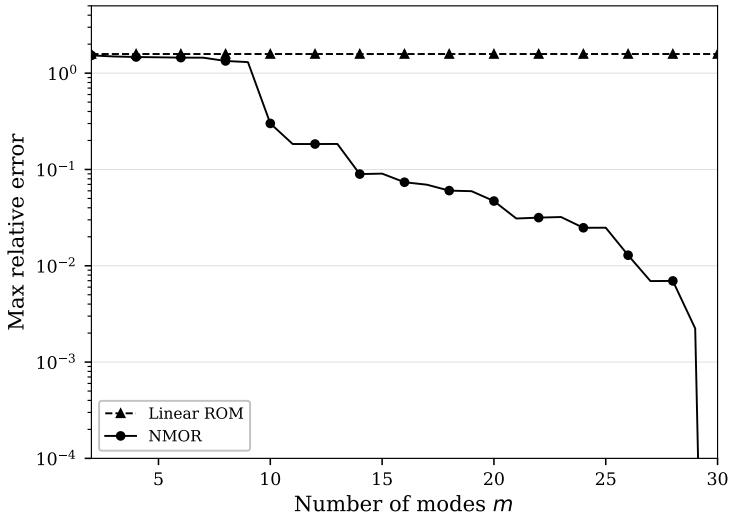

Figure 10: ROM convergence: linear ROM (no convergence) vs. NMOR (monotonic convergence) as a function of the number of modes m. $K_{nl} = 10^8$, $A = 0.01$.

Table 3: Computational performance: FOM vs. ROM with $m = 15$ modes (5000 time steps, $\Delta t = 10^{-4}$ s).

Case	t_{FOM} (s)	t_{NMOR} (s)	Speedup	$\varepsilon_{\mathrm{LROM}}$	$\varepsilon_{\mathrm{NMOR}}$
Moderate ($K_{nl} = 10^7$)	0.374	0.184	2.0×	1.672	0.006
Strong ($K_{nl} = 5 \times 10^7$)	0.405	0.187	2.2×	1.811	0.098
Extreme ($K_{nl} = 10^8$)	0.404	0.187	2.2×	1.581	0.091
Extreme, high amp ($K_{nl} = 10^8$, $A = 0.02$)	0.405	0.197	2.1×	1.829	1.472

the eigenvector phases can be factored out; for non-proportionally damped or aeroelastic systems [Tantaroudas and Da Ronch, 2017, Da Ronch et al., 2012], the unitary extension is essential.

3. Taylor-series convergence. For cubic nonlinearity, only the third-order Taylor operator $\boldsymbol{C}$ is non-trivial ($\boldsymbol{B} = 0$). The ROM with cubic correction captures amplitude-dependent phenomena with 15 reduced coordinates versus 30 full-order states, achieving order-of-magnitude accuracy improvement over the linear ROM. Extension to non-polynomial nonlinearities would require higher-order Taylor terms [Tantaroudas, 2015, Benner et al., 2015].

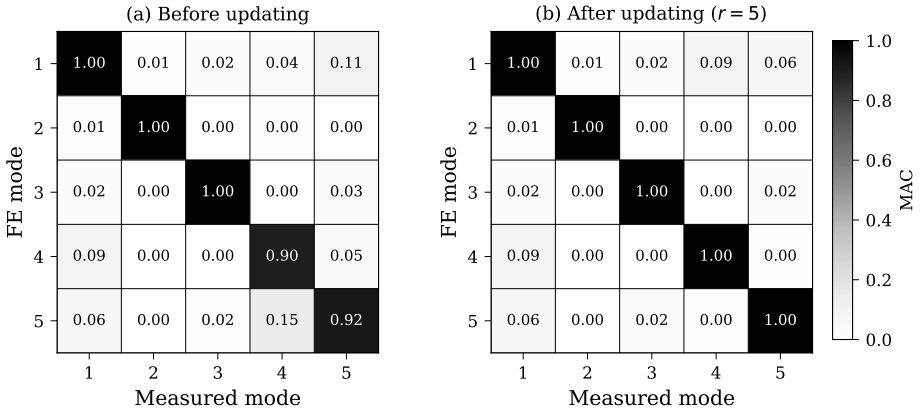

Figure 11: MAC matrices before (left) and after (right) linear model updating.

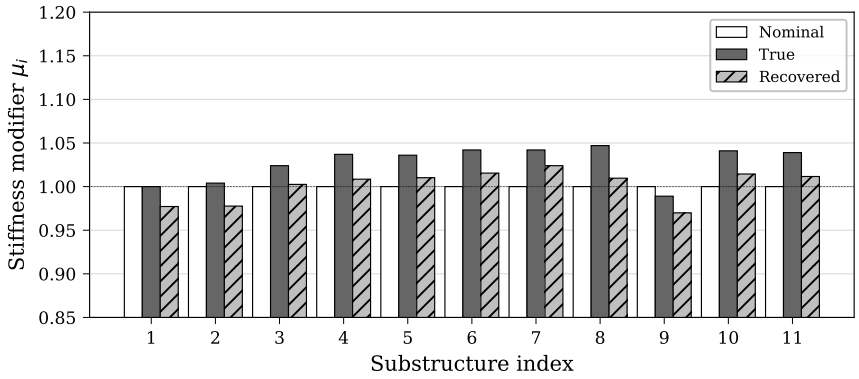

Figure 12: Comparison of true and recovered stiffness modifiers.

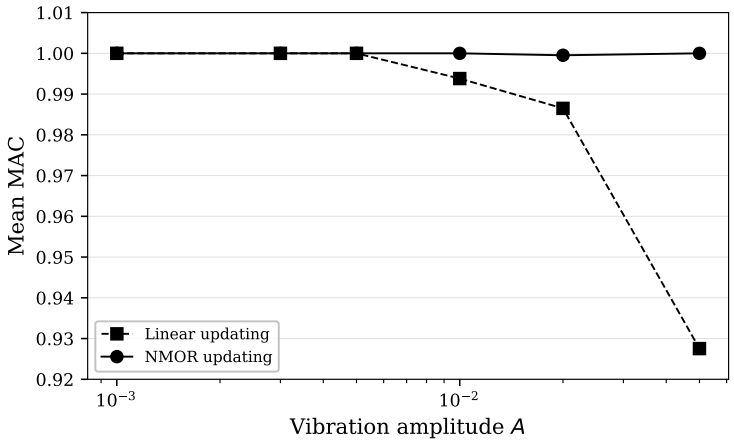

Figure 13: Mean MAC value vs. vibration amplitude: linear (Hollins) vs. NMOR (proposed) updating.

8 Conclusions

We have presented a nonlinear model-updating framework that combines the Taylor-series-based NMOR of Tantaroudas [2015] with the projection-basis adaptation scheme of Hollins et al. [2026]. The key contributions are:

1. A first-order state-space formulation of the wingbox structural model with Rayleigh damping and cubic stiffness nonlinearity.

2. Taylor-series expansion of the nonlinear restoring forces projected onto the biorthogonal eigenvector basis of the damped Jacobian, yielding a compact nonlinear ROM.

3. Generalisation of the Cayley-transform basis adaptation from the real orthogonal group to the unitary group.

4. Numerical demonstration that the NMOR-based updating captures amplitude-dependent natural frequencies and MAC values that a linear scheme cannot reproduce, with a order-of-magnitude reduction in time-domain prediction error.

Future work will apply this framework to: (a) experimental data from the physical wingbox panel with intentionally introduced nonlinear elements; (b) aeroelastic systems where the Jacobian is inherently non-symmetric and complex-valued due to aerodynamic coupling [Tantaroudas et al., 2015, 2014]; (c) higher-order Taylor expansions for non-polynomial nonlinearities.

Acknowledgements

The authors acknowledge Dr. Jake Hollins and the co-authors of Hollins et al. [2026] for making the wingbox experimental data and methodology available.

References

Jake Hollins, Tinkle Chugh, Evangelos Papatheou, Keith Worden, Konstantinos Tatsis, and Konstantinos Agathos. A projection basis adaptation scheme for the update of reduced order models using vibration measurements. *Mechanical Systems and Signal Processing*, 244:113796, 2026. doi:10.1016/j.ymssp.2025.113796.

Michael I. Friswell and John E. Mottershead. *Finite Element Model Updating in Structural Dynamics*. Springer, Dordrecht, 1995. doi:10.1007/978-94-015-8508-8.

John E. Mottershead, Michael Link, and Michael I. Friswell. The sensitivity method in finite element model updating: A tutorial. *Mechanical Systems and Signal Processing*, 25(7):2275–2296, 2011. doi:10.1016/j.ymssp.2010.10.012.

Randall J. Allemang. The modal assurance criterion – twenty years of use and abuse. *Sound and Vibration*, 37(8): 14–23, 2003.

Arthur Cayley. Sur quelques propriétés des déterminants gauches. *Journal für die reine und angewandte Mathematik*, 32:119–123, 1846.

Gaëtan Kerschen, Keith Worden, Alexander F. Vakakis, and Jean-Claude Golinval. Past, present and future of nonlinear system identification in structural dynamics. *Mechanical Systems and Signal Processing*, 20(3):505–592, 2006. doi:10.1016/j.ymssp.2005.04.008.

Keith Worden and Geoffrey R. Tomlinson. *Nonlinearity in Structural Dynamics: Detection, Identification and Modelling*. Institute of Physics Publishing, Bristol, 2001. ISBN 9780750303569.

Nikolaos D. Tantaroudas. *Nonlinear Model Order Reduction for Aeroelastic Systems*. PhD thesis, University of Liverpool, 2015.

N.D. Tantaroudas, A. Da Ronch, G. Gai, K.J. Badcock, and R. Palacios. An adaptive aeroelastic control approach using non linear reduced order models. In *14th AIAA Aviation Technology, Integration, and Operations Conference*, AIAA Paper 2014-2590, Atlanta, Georgia, 2014. doi:10.2514/6.2014-2590.

E. Papatheou, N.D. Tantaroudas, A. Da Ronch, J.E. Cooper, and J.E. Mottershead. Active control for flutter suppression: an experimental investigation. In *International Forum on Aeroelasticity and Structural Dynamics*, IFASD Paper 2013-8D, Bristol, U.K., 2013.

A. Da Ronch, N.D. Tantaroudas, S. Timme, and K.J. Badcock. Model reduction for linear and nonlinear gust loads analysis. In *54th AIAA/ASME/ASCE/AHS/ASC Structures, Structural Dynamics, and Materials Conference*, AIAA Paper 2013-1492, Boston, MA, 2013. doi:10.2514/6.2013-1492.

N.D. Tantaroudas, A. Da Ronch, K.J. Badcock, and R. Palacios. Model order reduction for control design of flexible free-flying aircraft. In *AIAA Atmospheric Flight Mechanics Conference, AIAA SciTech 2015*, AIAA Paper 2015-0240, Kissimmee, FL, 2015. doi:10.2514/6.2015-0240.

N.D. Tantaroudas and A. Da Ronch. *Nonlinear Reduced-order Aeroservoelastic Analysis of Very Flexible Aircraft*, chapter 4, pages 143–179. John Wiley & Sons, Ltd, Chichester, 2017. ISBN 9781118928691. doi:10.1002/9781118928691.ch4.

Cyril Touzé and Marco Amabili. Nonlinear normal modes for damped geometrically nonlinear systems: Application to reduced-order modelling of harmonically forced structures. *Journal of Sound and Vibration*, 298(4–5):958–981, 2006. doi:10.1016/j.jsv.2006.06.032.

Marc P. Mignolet, Adam Przekop, Stephen A. Rizzi, and S. Michael Spottswood. A review of indirect/non-intrusive reduced order modeling of nonlinear geometric structures. *Journal of Sound and Vibration*, 332(10):2437–2460, 2013. doi:10.1016/j.jsv.2012.10.017.

Ali H. Nayfeh and Dean T. Mook. *Nonlinear Oscillations*. John Wiley & Sons, 2008. ISBN 9783527617593.

Alan Edelman, Tomás A. Arias, and Steven T. Smith. The geometry of algorithms with orthogonality constraints. *SIAM Journal on Matrix Analysis and Applications*, 20(2):303–353, 1998. doi:10.1137/S0895479895290954.

Andrea Da Ronch, Ken J. Badcock, Yue Wang, Andrew Wynn, and Rafael Palacios. Nonlinear model reduction for flexible aircraft control design. In *53rd AIAA/ASME/ASCE/AHS/ASC Structures, Structural Dynamics and Materials Conference*, AIAA Paper 2012-4404, 2012. doi:10.2514/6.2012-4404.

Peter Benner, Serkan Gugercin, and Karen Willcox. A survey of projection-based model reduction methods for parametric dynamical systems. *SIAM Review*, 57(4):483–531, 2015. doi:10.1137/130932715.